AMERICAN JOURNAL OF PHYSIOLOGY
HEART AND CIRCULATORY PHYSIOLOGY

Am J Physiol Heart Circ Physiol 328: H885–H899, 2025.
First published March 4, 2025; doi:10.1152/ajpheart.00696.2024

RESEARCH ARTICLE

RNA Biology in the Cardiovascular System

Involvement of microRNA-146a-5p, but not -155-5p and -29b-5p, in left ventricular remodeling and dysfunction in spontaneously hypertensive rats

Siluleko A. Mkhize,[1] Sulé Gunter,[1,2] Ashmeetha Manilall,[1] Lebogang Mokotedi,[1,3] Kgotso L. Mosoma,[1] Refentshe Nthlane,[1] Aletta M. E. Millen,[1] and Frederic S. Michel[1]

[1]*Integrated Molecular Physiology Research Initiative, Department of Physiology, School of Biomedical Sciences, Faculty of Health Sciences, University of the Witwatersrand, Johannesburg, South Africa;* [2]*Department of Health Sciences and Medicine, Bond University, Gold Coast, Queensland, Australia; and* [3]*Department of Physiology, School of Medicine, Sefako Makgatho Health Sciences University, Ga-Rankuwa, South Africa*

Abstract

The contribution of microRNAs remains poorly understood in the context of hypertensive cardiac pathology. The role of miR-146a-5p, miR-155-5p, and miR-29b-5p in cardiac hypertrophy and dysfunction was investigated in spontaneously hypertensive rats (SHRs). Seven-month-old SHR ($n = 7$ male, $n = 9$ female) and normotensive Wistar Kyoto rats (WKY; $n = 7$ male, $n = 9$ female) underwent echocardiography. Plasma concentrations of inflammatory markers were measured by ELISA. Interstitial and perivascular fibrosis and percentage macrophage infiltration were determined by histology. Left ventricular (LV) mRNA expressions of cardiac remodeling markers and miRNA expressions were determined by RT-PCR. Circulating vascular cell adhesion molecule-1 (VCAM-1), macrophage infiltration, interstitial and perivascular fibrosis, relative wall thickness (RWT), early diastolic mitral inflow to tissue lengthening velocity at lateral mitral annulus (E/e′), and LV mRNA expression of *NFKBIA* and *SOD2* were greater in SHRs. MidFS, e′, and a′ were lower in SHRs. Expression of *LOX1*, *Col1a/Col3a* ratio, circulating c-reactive protein (CRP), interleukin-6 (IL-6), and tumor necrosis factor-alpha (TNF-α), and RWT were greater in females. No difference in miR-29b-5p expression was noted. MiR-155-5p expression was lower in female and associated with stroke volume and absolute heart and LV masses. MiR-146a-5p expression was greater in SHRs and associated with systolic blood pressure (SBP), circulating VCAM-1, macrophage infiltration, interstitial fibrosis, normalized heart and LV masses, RWT, and a'. MiR-146a-5p was also associated with circulating VCAM-1 after adjustments for SBP. In addition, greater expression of miRNA-146a-5p reversed the relationship between circulating VCAM-1 and macrophage infiltration. Changes in the expression of miR-155-5p may be involved with a cardiac phenotype related to sexual dimorphism. Conversely, upregulation of miR-146a-5p expression may act as a countermechanism induced by myocardial inflammation in the setting of reactive fibrosis, established LV hypertrophy, and impaired diastolic function.

NEW & NOTEWORTHY We investigated roles of microRNAs-146a-5p, -155-5p, and -29b-5p in development of cardiac hypertrophy and dysfunction in SHRs. We showed that miR-146a-5p expression was upregulated in SHRs and positively associated with indices of concentric LVH and diastolic dysfunction, potentially as countermechanism in response to myocardial inflammation, whereas miR-155-5p was expressed in a manner consistent with sexual dimorphism. Our data may offer novel insights on involvement of miRNAs in myocardial inflammation in hypertension-induced cardiac hypertrophy and dysfunction.

cardiac dysfunction; fibrosis; hypertension; inflammation; microRNAs

INTRODUCTION

The mechanisms involved in hypertension-induced cardiac remodeling and the associated dysfunctions remain an important area of research (1). The progression from hypertension to heart failure is driven by multiple pathological mechanisms, resulting in marked phenotypic heterogeneity (2). Nevertheless, it is well accepted that an increased afterload results in left ventricular hypertrophy (LVH), which is independently associated with the development of heart failure (3). In light with phenotypic heterogeneity, sex differences have been observed in the development, progression, and manifestation of hypertension-induced heart failure (4–6). In this regard, heart failure with preserved ejection fraction is more prevalent in women (2, 7, 8), whereas heart failure with reduced ejection fraction is more common in

Correspondence: S. A. Mkhize (siluleko.mkhize@wits.ac.za).
Submitted 8 October 2024 / Revised 13 November 2024 / Accepted 26 February 2025

men (7). This sexual dimorphism extends beyond anatomical variances and encompasses diverse physiological, hormonal, and genetic factors that influence cardiac function and pathology (9–11). Although the underlying mechanisms have been described in the literature, less is known about the upstream translational regulation of genes involved in the molecular pathways that govern the phenotypic expression of cardiac remodeling and dysfunction.

Recent work points to the unique contribution of noncoding RNAs (ncRNAs) (12–14). Of the ncRNAs, microRNAs (miRNAs) have received particular attention, due to their involvement in various pathophysiological conditions. In fact, the 2024 Nobel Prize in Physiology or Medicine, awarded jointly to Victor Ambros and Gary Ruvkun, highlights the critical role of miRNAs in posttranscriptional gene regulation. MiRNAs are small ncRNAs, ∼22 nucleotides long, that posttranscriptionally regulate gene and protein expression by binding to the 3′ untranslated region of target mRNA, thereby modulating its translation (15). In this regard, dysregulated miRNA expression patterns have been associated with various pathophysiological mechanisms in cardiac remodeling and dysfunction (16), including myocardial fibrosis (17), inflammation (18), and oxidative stress (18–22).

In rodent models of pressure overload, miRNAs have been shown to regulate genes that modulate the development of concentric LVH and myocardial dysfunction (12). The aberrant expression of miRNAs has been linked to the development of concentric LVH (23–26). In particular, miR-146a-5p (26), miR-29b-5p (23), and miR-155-5p (27) may play a role in regulating gene expression, influencing the development of concentric LVH and myocardial dysfunction. Specifically, miR-146a-5p was upregulated after transverse aortic constriction (TAC) or angiotensin-II administration in combination with isoproterenol (18). In patients with aortic stenosis, miR-146a-5p was significantly upregulated and positively associated with increased LV wall thickness, an index of LVH (18). In male mice subjected to TAC, miR-29b-5p was downregulated (17) but upregulated in female mice. In streptozotocin-induced diabetic cardiomyopathy, miR-146a-5p was also downregulated (28), with no indications of sexually dimorphic features. Conversely, miR-29b-5p was upregulated in female rats after pressure overload, suggesting that miRNAs may have sex-specific effects on cardiac function (17). Studies have indicated that miR-155-5p may be upregulated in females with inflammatory conditions (29), whereas miR-146a-5p, which plays a role in inflammation and immune response, could also exhibit sex differences in its regulation (30). However, these findings are context-dependent and seem to vary across tissues and disease states.

Taken together, these findings indicate that miR-146a-5p, miR-29b-5p, and miR-155-5p may be key regulators in cardiac remodeling and dysfunction. Yet, to the best of our knowledge, their contribution to hypertensive cardiac pathology remains poorly described. The spontaneously hypertensive rat (SHR) is a well-established genetic model that closely recapitulates the milieu associated with the development and consequences of human essential hypertension (5). The SHR model may therefore be the most appropriate model to study the relative contribution of ncRNAs in adverse cardiac remodeling and dysfunction. We, therefore, investigated the patterns of expression and involvement of miR-146a-5p, -155-5p, and -29b-5p in male and female SHRs with established concentric LVH.

METHODS

Animals and Housing

We obtained approval from the Animal Ethics Screening Committee of the University of the Witwatersrand, Johannesburg, South Africa (Clearance number: 2021/03/03 C), and adhered to the National Institutes of Health Guide for the Care and Use of Laboratory Animals, as well as the Animal Research: Reporting of In vivo Experiments (ARRIVE) guidelines (31). Animals were housed individually in controlled ambient temperature conditions with a 12-h light-dark cycle and provided ad libitum access to drinking water, and standard laboratory animal chow (Labchef, Johannesburg, South Africa). Colored balls and tunnels were provided for environmental enrichment.

Study Design

Seven-month-old spontaneously hypertensive rats (SHRs, $n = 7$ male, $n = 9$ female, RRID: RGD_10043828) and normotensive Wistar Kyoto rats (WKY, $n = 7$ male and $n = 9$ female, RRID: RGD_61119) were obtained from and housed at the Wits Research Animal Facility (WRAF). Both sexes were used in the present study because evidence of a sexual dimorphism in arterial blood pressure and adverse cardiovascular outcomes have been shown in SHRs (6, 9–11, 32); however, we did not evaluate the estrous cycle in female rats. For a period of 2 wk, the rats were acclimatized to handling the housing environment. Sample size estimation was determined based on the previous studies (6, 9–11, 32). In brief, an a priori sample size calculation using a two-way analysis of variance (ANOVA) test, with an α of 0.05 and 80% power, indicated that a total of 32 rats ($n = 7$–9 per group) would be adequate to detect statistical differences in this model (G*Power, v. 3.1.9.2).

Noninvasive Blood Pressure Measurement

Before termination, blood pressure (BP) was measured in all rats. In brief, the tail-cuff technique was employed using noninvasive BP (NIBP) amplifiers (Biopac Systems Inc., Santa Barbara, RRID:SCR_014829). To obtain BP readings, conscious rats were placed in a restrainer with the tail lassoed with a BP cuff and placed on a thermostatic blanket (adjusted to 37°C) according to a previously described protocol (33). Rats were habituated before the first measurement to enable them to adapt to the restrainer and BP measurement protocol. Measurements were taken at midday to avoid diurnal variations in BP.

Transthoracic Echocardiography

Rats were anesthetized with isoflurane (5% for induction, and thereafter maintained at 1%–2.5% concentration via 100% O_2 mask inhalation). Under anesthesia, echocardiography was performed using a noninvasive high-resolution (paediatric-10 MHz) ultrasound probe connected to an echocardiogram (Siemens, Acuson SC2000, Diagnostic ultrasound system; Siemens Medical Solutions, Inc.). In the parasternal long-axis view of the LV, LV dimensions, including LV

internal diameter in systole (LVIDs), left ventricular internal diameter in diastole (LVIDd), interventricular septal thickness in systole (IVSTs), interventricular septal thickness in diastole (IVSTd), LV posterior wall thickness in systole (LVPWTs), and LV posterior wall thickness in diastole (LVPWTd), were measured from M-mode echocardiography. Indices of LV systolic function were derived from the LV dimensions. Stroke volume was calculated using the Teichholz method (7). The ejection fraction was computed as EF = [(LVEDV − LVESV)/LVEDV] × 100, where LVEDV and LVESV are the LV end-diastolic volume and LV end-systolic volume, respectively. Endocardial fractional shortening (endFS) was computed as endFS = (LVIDd − LVIDs)/LVIDd × 100. Midwall fractional shortening (midFS) was determined as midFS = [(LVIDd + PWTd) − (LVIDs + PWTs)]/[(LVIDd + PWTd)] × 100. LV relative wall thickness (RWT) was calculated as RWT = (2 × PWTd)/LVIDd (7).

LV diastolic function was evaluated via pulsed Doppler imaging to ascertain mitral valve inflow patterns. In brief, in the apical four-chamber view, early (E) and late (A) diastolic inflow velocities were recorded with the sample volume positioned at the tip of the mitral valve leaflet, and the E, A, and E/A ratio were calculated as indices of relaxation. Tissue Doppler imaging (TDI) was used to assess peak myocardial tissue lengthening velocities during early (e′) and late (a′) diastole recorded at the level of the lateral mitral annulus in the apical four-chamber view. Data are expressed as e′, an index of myocardial relaxation, e′/a′, an index of myocardial stiffness, and E/e′ representing LV filling pressure (33).

Echocardiographic assessment was conducted by a trained sonographer who was blinded to the experimental groups. All assessments were conducted in accordance with the American Society of Echocardiography guidelines (34).

Blood and Tissue Sampling

After echocardiography, a thoracotomy was performed and rats were exsanguinated via cardiac puncture. Blood was collected into sterile EDTA tubes for plasma, centrifuged, and stored at −80°C for subsequent analysis. The organs were excised and weighed. LV tissue was divided and either preserved in 10% buffered formalin for histological analysis or in RNAlater (Ambion; Sigma-Aldrich, Germany), an RNA stabilizing reagent, to ensure RNA integrity in postmortem tissue samples for reliable gene expression analysis.

Circulating Levels of Inflammatory Markers

A cassette of plasma concentrations of the inflammatory markers including c-reactive protein (CRP), tumor necrosis factor-alpha (TNF-α), interleukin-6 (IL-6), and vascular cell adhesion molecule-1 (VCAM-1) were determined using commercially available solid-phase sandwich enzyme-linked immunosorbent assay (ELISA) kits (Elabscience Biotechnology, Co Ltd, Wuhan, PR China). Each sample was run in duplicate, with TNF-α, IL-6, CRP, and VCAM-1 exhibiting lower detection limits of 78.13 pg/mL, 62.50 pg/mL, 0.31 ng/mL, and 12.5 pg/ml, respectively. All measurements had coefficients of variation <10%.

Myocardial Macrophage Infiltration

LV tissue samples that were preserved in 10% buffered formalin underwent standard procedures for embedding in paraffin. Thin (5-μm) sections were prepared from the embedded tissues using a microtome and then subjected to deparaffinization and rehydration (33). Thereafter, the tissue sections were stained with hematoxylin and eosin (H&E) to visualize nuclei and cytoplasm, respectively. Following staining, the slides were rinsed in acidified water, dehydrated, and mounted using a digital picture exchange (DPX) mounting medium. Examination of the tissue sections was performed using a Zeiss Axioscope 2 Plus microscope equipped with a Zeiss AxioCam (Zeiss, Peabody, MA, RRID: SCR_023747). Macrophages were identified based on their distinct morphology, including round to oval shapes, abundant eosinophilic cytoplasm, and large, eccentrically placed nuclei.

Perivascular and Myocardial Collagen Content

LV tissue sections were stained using a 0.1% Sirius red solution dissolved in a saturated picric acid solution for 60 min at ambient temperature. Following staining, the slides were rinsed in acidified water, dehydrated, and mounted using a digital picture exchange (DPX) mounting medium. Examination of the tissue sections was performed using a Zeiss Axioscope 2 Plus microscope equipped with a Zeiss AxioCam (Zeiss, Peabody, MA, RRID:SCR_023747). The sections were visualized under bright-field using a ×10 objective lens. Utilizing ImageJ software (RRID:SCR_003070), the myocardial collagen fraction area was determined for each tissue section by dividing the area occupied by collagen by the total tissue area (33). Perivascular collagen content of the coronary vessels was quantified as the total area stained with Sirius red and expressed as a percentage of the total tissue section.

Total RNA Isolation

Total RNA was extracted from LV tissue using an Illustra RNAspin Mini Isolation kit (GE Healthcare, Buckinghamshire) according to the manufacturer's instructions. The quality and quantity of RNA were confirmed using a Nanodrop OneC spectrophotometer (Thermo Fisher Scientific, Waltham). The RNA was then reverse-transcribed using SuperScript IV VILO cDNA Synthesis Master Mix (Thermo Fisher Scientific, Waltham). The quality and quantity (>1,000 ng/μL) of cDNA were again confirmed using a Nanodrop OneC spectrophotometer (Thermo Fisher Scientific, Waltham). The cDNA products were stored at −20°C for further analyses.

Expression of Target Genes

Comparative gene expression RT-PCR was performed using the cDNA (∼2 μg), predesigned TaqMan probe mixes for the reference gene hypoxanthine guanine phosphoribosyl transferase (*HPRT1*, 0.25 μL, TaqMan assay ID: Rn01527838_g1; Thermo Fisher Scientific, Life Technologies, Carlsbad), the gene of interest (0.5 μL, TaqMan gene expression assay), and TaqMan Fast Advanced PCR master mix (5 μL) in a final volume of 10 μL. Comparative gene expression of *Col1a* mRNA, which codes for Collagen type-I (TaqMan assay ID: Rn01463848_m1), *Col3a* mRNA, which codes for Collagen type-III (TaqMan assay ID: Rn01437681_m1), *LOX1* mRNA, which codes for lysyl oxidase 1 (TaqMan assay ID: Rn01463024_g1), *NFKBIA* mRNA, which codes for the nuclear factor of kappa light polypeptide gene

enhancer in B-cells inhibitor alpha (commonly abbreviated as IκBα, TaqMan assay ID: Rn01473657_g1), *IL-1β* mRNA, which codes for inteleukin-1β (TaqMan assay ID: Rn00676333_g1), *PTX-3* mRNA, which codes for pentraxin-3 (TaqMan assay ID: Rn01769850_m1), *RUNX-1* mRNA, which codes for runt-related transcription factor 1 (TaqMan assay ID: Rn01645281_m1), and *SOD2* mRNA, which codes for superoxide dismutase 2 (TaqMan assay ID: Rn00690588_g1) were all determined in duplex reactions with the endogenous control probe *HPRT1*, in duplicated plates. The relative expression of each gene of interest was calculated using the $2^{-\Delta\Delta Ct}$ method (35).

MicroRNA Expression

The cDNA templates were used for microRNA expression analyses by comparative expression RT-PCR. Here, three (3) candidate endogenous control probes, including small nuclear RNA (SnU6, TaqMan assay ID: 002299), miR-16-5p (TaqMan assay ID: rno481312_miR), and miR-191-5p (TaqMan assay ID: rno480971_miR), were tested across a subset of samples that represented all experimental groups (7 per group, $n = 28$ in total). The most suitable endogenous control was selected using RefFinder (RRID: SCR_000472). MiR-191-5p proved to be expressed with the least variability across all samples and between experimental groups, with a distinguishably low standard deviation in cycle threshold values, and was therefore considered as the most reliable reference gene for the remaining microRNA analyses.

Thereafter, commercially available microRNA TaqMan probes were used to analyze microRNA expression, including miR-29b-5p (TaqMan assay ID: rno481033_miR), -146a-5p (TaqMan assay ID: rno481451), and -155-5p (TaqMan Assay ID: rno480953_miR). Each well of a 96-well plate comprised a total volume of 20 μL consisting of 5 μL of cDNA template, 10 μL of TaqMan Fast Advanced Master Mix (2×), 1 μL TaqMan Advanced microRNA Assay (20×) (Thermo Fisher Scientific, Waltham), and 4 μL of RNase-free water. Each sample was assayed in duplicate reactions. The reaction plate was loaded into the StepONE Plus real-time PCR instrument (Thermo Fisher Scientific, Waltham). The $2^{-\Delta\Delta Ct}$ method was used to calculate the microRNA expression relative to the expression of the endogenous reference control, miR-191-5p (TaqMan assay ID: rno480971_miR) (35). The miRNAs selected for our study were based on the literature, where we identified candidates that were previously implicated in cardiovascular processes relevant to our research. Thereafter, in silico analysis using TargetScan (http://www.targetscan.org/vert_80/) and MiRDB (http://www.mirdb.org/) were conducted to identify their putative targets. TargetScan and miRDB are computational tools that predict putative miRNA targets by identifying conserved 8mer, 7mer, and 6mer sites matching the seed regions of miRNAs.

Statistical Analyses

Statistical analyses were performed using the STATA software, version 16.1 (STATA Institute Inc., College Station, TX). Visualizations were performed using GraphPad Prism version 10.3.1 for Windows (GraphPad Prism, MA, RRID:SCR_002798). Data are expressed as arithmetic means ± standard deviation (SD). Group differences were determined by two-way analysis of variance (2-way ANOVA) test with strain (WKY vs. SHR) and sex (male vs. female) as the main effects. Following the 2-way ANOVA, Tukey's post hoc tests were conducted to correct for multiple comparisons. Bivariate correlations were determined using Pearson's correlation analyses and presented as a volcano plot. For dimensionality reduction, a principal component analysis (PCA) was conducted using the FactoMineR and factoextra packages in RStudio using the R programming language [R Core Team (2021)] accessed via the R Foundation for Statistical Computing, Vienna, Austria (https://www.R-project.org/). First, the data were standardized (mean = 0, SD = 1) to ensure comparability across variables. The PCA produced eigenvalues and proportions of variance for 35 components. A scree plot was generated to visualize the eigenvalues, and the contribution of variables to the principal components was assessed. As a visual heuristic, the scree plot determined that the first two principal components captured most of the variance in the dataset using the elbow method. A biplot was constructed to ascertain whether there was significant clustering in the PCA scores when disaggregated by sex. A permutational multivariate analysis of variance (PERMANOVA) test utilizing the Euclidean method was performed to categorically examine whether there were significant sex-specific differences in the PCA scores using the vegan package.

In multivariable analyses, interaction terms were created to assess whether the relationship between VCAM-1 and macrophage infiltration was moderated by miR-146a-5p or systolic blood pressure (SBP). Before the analysis, data were filtered to include only rows with nonmissing and finite values for VCAM-1, miR-146a-5p, and SBP. Thereafter, a multivariable linear regression model with three-way interaction terms was run. The final model included the main effects of VCAM-1, miR-146a-5p, and SBP, along with their two-way interaction terms, and a Wald chi-squared test was performed to compare the coefficients of the slopes. To visualize the interaction effects, a prediction dataset was generated using a grid of VCAM-1 values ranging from its observed minimum to maximum. MiR-146a-5p and SBP were each set at their mean, as well as one standard deviation above and below the mean, capturing low, medium, and high levels of these variables. Predicted macrophage infiltration values were obtained using the fitted model, and results visualized using an interaction plot. Statistical significance was considered at $P < 0.05$.

RESULTS

Systolic and Diastolic Blood Pressure

Systolic BP (Table 1) was significantly higher in SHR compared with WKY ($P < 0.0001$). A significant interaction ($P < 0.0003$) was noted for diastolic BP (Table 1). Diastolic BP was significantly higher in female SHR compared with the other three experimental groups (all $P < 0.0001$).

Body and Organ Masses

WKY were significantly heavier than SHRs ($P < 0.0001$, Table 1). Male rats were significantly heavier compared with their female counterparts ($P < 0.0001$). The heart and LV mass of SHRs were significantly greater than that of normotensive WKY rats ($P = 0.008$ and $P = 0.001$, respectively). In

Table 1. *Body and organ masses of male and female WKY and SHRs*

	Male		Female		*P* Value		
	WKY (n = 7)	SHR (n = 7)	WKY (n = 9)	SHR (n = 9)	Strain	Sex	Interaction
Hemodynamic							
SBP, mmHg	130 ± 4	171 ± 11	126 ± 6	171 ± 5	**<0.0001**	0.401	0.331
DBP, mmHg	89 ± 3	95 ± 4	89 ± 3	107 ± 6###†⁋	**<0.0001**	**0.001**	**0.0003**
Gravimetric							
Body mass, g	389 ± 15	355 ± 28	240 ± 23	202 ± 11	**<0.0001**	**<0.0001**	0.788
Heart mass, g	1.28 ± 0.08	1.48 ± 0.15$¥	0.94 ± 0.10***	0.95 ± 0.09###$	**0.008**	**<0.0001**	**0.022**
Heart mass, g/100 g	0.33 ± 0.02	0.41 ± 0.03	0.39 ± 0.03	0.47 ± 0.04	**<0.0001**	**<0.0001**	0.794
LV mass, g	0.85 ± 0.10	1.11 ± 0.17$¥	0.67 ± 0.08*	0.68 ± 0.07###$	**0.001**	**<0.0001**	**0.003**
LV mass g/100 g	0.22 ± 0.02	0.31 ± 0.03	0.28 ± 0.03	0.34 ± 0.03	**<0.0001**	**0.0002**	0.119
Kidney mass, g	1.39 ± 0.09	1.32 ± 0.15	0.87 ± 0.08	0.78 ± 0.04	**0.016**	**<0.0001**	0.698
Kidney mass, g/100 g	0.36 ± 0.01	0.37 ± 0.04	0.36 ± 0.02	0.38 ± 0.03	0.071	0.323	0.777
Liver mass, g	9.97 ± 0.52	11.2 ± 1.33	6.94 ± 0.56	7.29 ± 1.12	**0.034**	**<0.0001**	0.232
Liver mass, g/100 g	2.56 ± 0.17	3.15 ± 0.35	2.89 ± 0.19	3.60 ± 0.49	**<0.0001**	**0.003**	0.646

Data expressed as means ± SD. Organ masses are normalized to body mass and expressed as g/100 g. Two-way ANOVA with Tukey's post hoc test. Boldface indicates statistically significant effects. DBP, diastolic blood pressure; LV, left ventricular; SBP, systolic blood pressure; SHR, spontaneously hypertensive rats; WKY, Wistar Kyoto rats. ***P < 0.0001 in WKY (male vs. female), ###P < 0.0001 in SHR (male vs. female), \$$P$ < 0.05 vs. WKY male, ¥P < 0.05 vs. WKY female, *P < 0.05 vs. WKY male, †P < 0.0001 vs. WKY male, and ⁋P < 0.0001 vs. WKY female.

addition, the heart and LV mass of male rats were significantly greater compared with those of female rats (P < 0.0001 for both). Similarly, the kidney and liver mass of WKY rats were significantly greater than those of SHRs (P = 0.016 and P = 0.034, respectively). The kidney and liver mass of male rats were significantly greater than those of female rats (P < 0.0001 for both). When normalized to body mass, the heart and LV mass of female rats were significantly greater than those of male rats (P < 0.0001 for both). The liver mass normalized to body mass was significantly greater in female compared with that in male rats (P = 0.003) and in SHR compared with WKY (P < 0.0001). The kidney mass normalized to body mass was not different between the different experimental groups (P > 0.05).

Left Ventricular Geometry, Diastolic, and Systolic Function

The LVIDs and LVPWTs were similar among all the groups (all P > 0.05, Table 2). The LVIDd of SHR was significantly reduced compared with that of WKY (P = 0.010). In addition, female rats had smaller LVIDd compared with male rats (P = 0.013). Female rats had smaller IVSTs and IVSTd compared with male rats (P = 0.007 and P = 0.027, respectively). The RWT of SHR was significantly greater compared with WKY (P = 0.0002) and exhibited that female rats had greater RWT compared with male rats (P = 0.043). Finally, the LVPWTd of SHR was significantly greater compared with that of WKY (P = 0.0003) but tended to be greater in female compared with male rats (P = 0.078). The e′/a′ and E/A ratios were similar among the groups (all P > 0.05, Table 2). The e′ and a′ were significantly lower in SHR compared with WKY (P = 0.003 and P = 0.0002, respectively). The E, A, and E/e′ ratios were significantly greater in SHR compared with WKY (P = 0.045, P = 0.034, and P = 0.011, respectively). No significant sex effect was noted for all indices of LV diastolic function (all P > 0.05). The endFS was similar among all the groups (all P > 0.05, Table 2). The midFS was greater in WKY compared with SHR (P = 0.011). Female rats exhibited lower midFS compared with male rats (P = 0.004). Ejection fraction was similar between the groups (P > 0.05). Stroke volume was decreased in SHR compared with WKY (P = 0.003) and also decreased in female rats compared with their male counterparts (P = 0.033).

LV Tissue-Specific Expression of MicroRNAs

LV tissue miR-146a-5p expression was greater in SHR compared with WKY (P < 0.0001) but similar between male and female rats (P = 0.805, Fig. 1*A*). Conversely, LV tissue miR-155-5p expression was lower in female rats compared with male rats (P = 0.012) but similar between WKY compared with SHR (P = 0.899, Fig. 1*B*). Finally, LV tissue miR-29b-5p expression was not different between all the experimental groups (all P > 0.05, Fig. 1*C*).

Circulating Concentrations of Inflammatory Markers

The circulating concentration of CRP did not differ between WKY and SHR (P = 0.559) but was greater in female compared with male rats (P = 0.022, Fig. 2*A*). The circulating concentrations of IL-6 (Fig. 2*B*) and TNF-α (Fig. 2*C*) were similar between WKY and SHR (P = 0.599 and P = 0.684, respectively) but were also greater in female compared with male rats (P = 0.011 and P < 0.0001, respectively). The circulating concentration of VCAM-1 was similar between male and female rats (P = 0.082) but was greater in SHR compared with WKY (P < 0.0001, Fig. 2*D*).

Macrophage Infiltration, Perivascular, and Myocardial Fibrosis in Left Ventricular Tissue

Myocardial macrophage infiltration was greater in SHR compared with WKY (P < 0.0001) but similar between male and female rats (P = 0.159) (Fig. 3*A*). Perivascular collagen deposition was also greater in SHR compared with WKY (P < 0.05) but similar between male and female rats (P = 0.280) (Fig. 3*B*). Myocardial collagen content expressed as a percentage of the total section was significantly greater in SHR compared with WKY (P = 0.016) but similar between male and female rats (P = 0.659) (Fig. 3*C*).

Gene Expression in Left Ventricular Tissue

In the left ventricular tissue, gene expression levels were analyzed across male and female WKY and SHR (Table 3). For

Table 2. *Echocardiographic parameters showing left ventricular geometry, diastolic, and systolic function in male and female normotensive WKY and SHR*

	Male		Female		*P* Value		
	WKY (n = 7)	SHR (n = 7)	WKY (n = 9)	SHR (n = 9)	Strain	Sex	Interaction
LV geometry							
LVIDs, cm	0.35 ± 0.09	0.35 ± 0.14	0.29 ± 0.06	0.31 ± 0.07	0.787	0.225	0.922
LVIDd, cm	0.68 ± 0.06	0.62 ± 0.08	0.61 ± 0.05	0.53 ± 0.09	**0.010**	**0.013**	0.930
IVSTs, cm	0.38 ± 0.09	0.37 ± 0.07	0.29 ± 0.04	0.30 ± 0.06	0.961	**0.007**	0.708
IVSTd, cm	0.27 ± 0.08	0.31 ± 0.11	0.21 ± 0.01	0.24 ± 0.06	0.210	**0.027**	0.867
LVPWTs, cm	0.28 ± 0.09	0.34 ± 0.06	0.31 ± 0.03	0.35 ± 0.06	0.056	0.381	0.566
LVPWTd, cm	0.19 ± 0.04	0.31 ± 0.09	0.24 ± 0.07	0.35 ± 0.06	**0.0003**	0.078	0.727
RWT	0.55 ± 0.16	1.03 ± 0.26	0.83 ± 0.26	1.14 ± 0.23	**0.0002**	**0.043**	0.375
LV diastolic function							
e′, cm/s	4.33 ± 1.03	3.29 ± 0.76	4.50 ± 1.64	3.00 ± 0.67	**0.003**	0.879	0.566
a′, cm/s	8.33 ± 2.58	3.57 ± 1.13	6.00 ± 3.52	3.60 ± 1.17	**0.0002**	0.170	0.160
e′/a′	0.54 ± 0.11	0.97 ± 0.28	1.15 ± 0.99	0.90 ± 0.31	0.636	0.177	0.088
E, cm/s	60 ± 19	155 ± 142	56 ± 26	107 ± 89	**0.045**	0.462	0.530
A, cm/s	26 ± 9	64 ± 45	27 ± 24	53 ± 48	**0.034**	0.740	0.706
E/A	2.43 ± 0.80	2.48 ± 0.98	2.79 ± 1.16	2.15 ± 1.07	0.458	0.970	0.387
E/e′	14 ± 5	46 ± 36	13 ± 5	35 ± 29	**0.011**	0.524	0.599
LV systolic function							
Stroke volume, mL	0.57 ± 0.19	0.36 ± 0.15	0.42 ± 0.12	0.26 ± 0.13	**0.003**	**0.033**	0.663
Ejection fraction, %	78 ± 11	82 ± 4	79 ± 8	69 ± 11	0.396	0.101	0.071
endFS, %	43 ± 12	45 ± 4	43 ± 9	34 ± 8	0.311	0.112	0.143
midFS, %	29 ± 5	23 ± 3	22 ± 8	17 ± 3	**0.011**	**0.04**	0.743

Data expressed as means ± SD. Two-way ANOVA with Tukey's post hoc test. Boldface indicates statistically significant effects. A, maximum late mitral inflow velocity; a′, late peak tissue lengthening velocity at lateral mitral annulus; E, maximum early mitral inflow velocity; E/A, early to late diastolic filling velocity ratio; E/e′, early diastolic mitral inflow to tissue lengthening velocity at lateral mitral annulus; e′, early peak tissue lengthening velocity at lateral mitral annulus; e′/a′, early to late peak tissue lengthening velocity ratio; endFS, endocardial fractional shortening; IVSTd, interventricular septal thickness in diastole; IVSTs, interventricular septal thickness in systole; LV, left ventricular; LVIDd, left ventricular internal diameter in diastole; LVIDs, left ventricular internal diameter in systole; LVPWTd, left ventricular posterior wall thickness in diastole; LVPWTs, left ventricular posterior wall thickness in systole; midFS, midwall fractional shortening; RWT, relative wall thickness; SHR, spontaneously hypertensive rats; WKY, Wistar Kyoto rats.

NFKBIA, expression was higher in SHRs than WKYs (P = 0.024), but no significant differences were observed for sex (P = 0.634) or interaction effects (P = 0.504). *IL-1β* showed no significant differences in strain (P = 0.301), sex (P = 0.849), or interaction (P = 0.240). *PTX-3* expression was significantly higher in females compared with males (P = 0.037) but showed no strain and interaction effects (P = 0.484 and P = 0.501, respectively). For fibrosis-related genes, *Col3a* showed no significant differences in strain (P = 0.655), sex (P = 0.941), or interaction (P = 0.428). *Col1a* expression was significantly higher in females compared with males (P < 0.0001), with no significant strain (P = 0.235) or interaction (P = 0.631) effects. Similarly, *Col1a/Col3a* ratio and *LOX1* were significantly higher in females than males (P = 0.0094 and P = 0.0006, respectively). *RUNX1*, related to apoptosis, was also significantly elevated in females (P = 0.0002), with no significant strain (P = 0.520) or interaction (P = 0.893) effects. Finally, *SOD2*, related to oxidative stress, showed higher expression in SHRs compared with WKYs (P = 0.001) but no significant differences by sex (P = 0.628) or interaction (P = 0.645).

Associations between microRNAs and Hemodynamic, Gravimetric, Echocardiographic, and Molecular Parameters

Figure 4 shows a volcano plot depicting associations between the three microRNAs (miR-146a-5p, miR-155-5p,

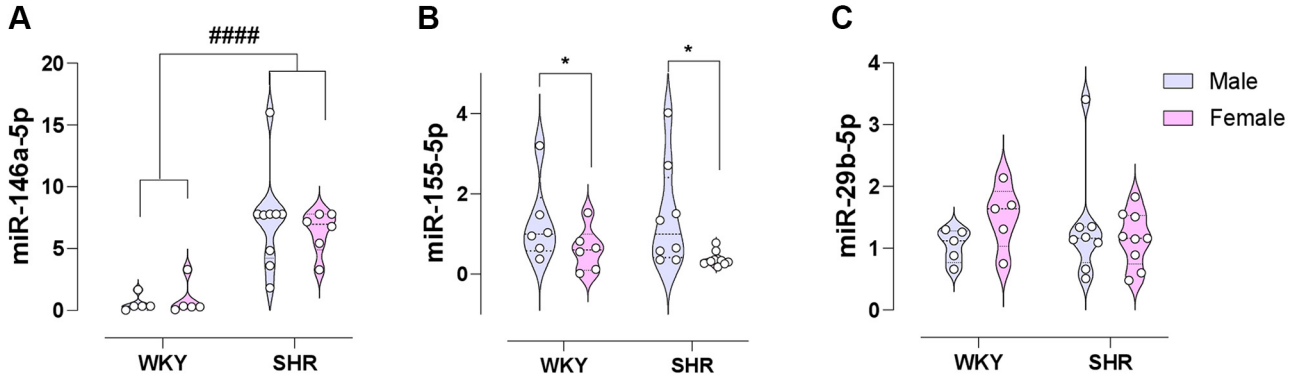

Figure 1. *A*–*C*: a violin plot illustrating heart tissue-specific expression of microRNAs relative to miR-191-5p as endogenous control including miR-146a-5p (*A*), miR-155-5p (*B*), and miR-29b-5p (*C*). Two-way ANOVA with Tukey's post hoc test. *P < 0.05, and ####P < 0.0001. SHR, spontaneously hypertensive rat; WKY, Wistar Kyoto rat.

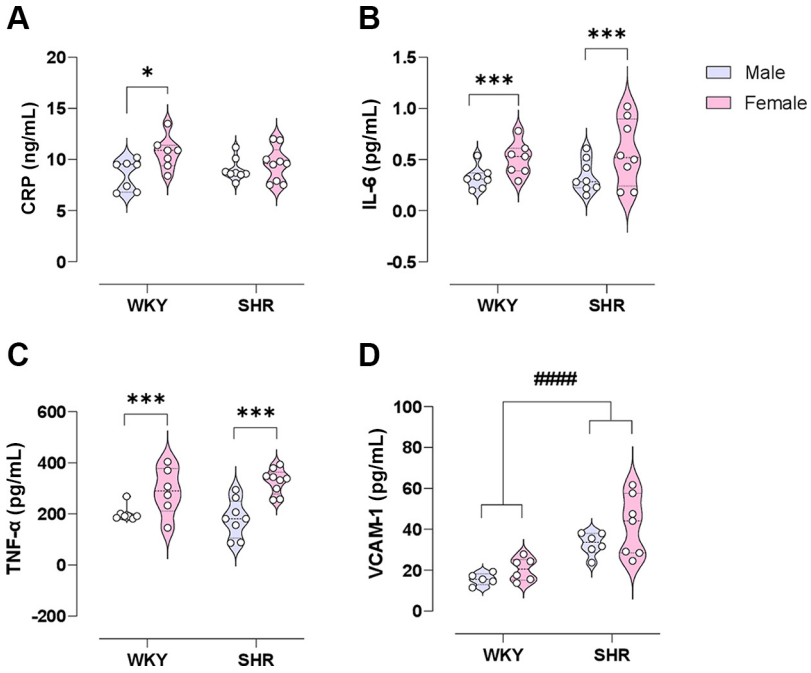

Figure 2. *A–D*: circulating concentrations of the proinflammatory markers C-reactive protein (CRP, *A*), interleukin-6 (IL-6, *B*), tumor necrosis factor-α (TNF-α, *C*), and vascular cell adhesion molecule-1 (VCAM-1, *D*) in male and female normotensive WKY and SHRs. Two-way ANOVA with Tukey's post hoc test. $*P < 0.05$, $***P < 0.0001$, and $\#\#\#\#P < 0.0001$. SHR, spontaneously hypertensive rat; WKY, Wistar Kyoto rat.

and miR-29b-5p) and cardiovascular parameters, gene expression in left ventricular tissue, and circulating concentrations of inflammatory markers. The *x*-axis displays Pearson's correlation coefficients (r), whereas the *y*-axis shows the $-\log_{10}(P$ value). Points above the horizontal dashed line [$-\log_{10}(P$-value) = 1.30, equivalent to $P = 0.05$] indicate statistically significant correlations. Red markers highlight significant positive correlations, particularly involving miR-146a-5p (e.g., SBP, RWT, LVIDd, LVPWTd, VCAM-1, myocardial fibrosis, macrophage infiltration, and normalized liver mass, LV mass, and heart mass). Parameters associated with miR-155-5p (e.g., absolute LV mass, kidney mass, heart mass, and stroke volume) are also highlighted in red. The turquoise marker represents a significant negative correlation between miR-146a-5p and e′ (cm/s). Although the expression of *NFKBIA* and *SOD2* was greater in SHR, their association with miR-146a-5p did not reach statistical significance (both $P > 0.05$). In multivariable analyses, miR-146a-5p was persistently associated with circulating concentrations of VCAM-1 independent of the confounding effect of SBP; β [95% CI]: 0.468 [0.033 to 0.902], $P = 0.040$. Table 4 presents the full suite of relationships between microRNAs and the various parameters.

Sexually Dimorphic Features

Figure 5*A* depicts the eigenvalue scree plot exhibiting principal component analysis (PCA). The first principal component (PC1) explains 25.7% of the total variance, indicating that it is the most important axis of variation in the dataset. The second principal component (PC2) explains 15.7% of the total variance. As such, including more components adds diminishing amounts of explained variance. For PC1, the most contributing variables include absolute kidney mass (4.67%), normalized heart mass (3.98%), and normalized left ventricular mass (3.24%). For PC2, important contributors include absolute heart (6.50%) and liver masses (7.12%). When disaggregated by sex, sample clustering was observed in the biplot (Fig. 5*B*) and a PERMANOVA test revealed highly significant sex-specific differences in PCA scores (Pillai's Trace = 0.71596, $P < 0.001$).

Moderation Effects of miR-146a-5p and Systolic Blood Pressure

The interaction plot (Fig. 6) illustrates the relationship between circulating concentrations of VCAM-1 and myocardial macrophage infiltration while considering the moderating effects of miR-146a-5p levels (colored lines) and SBP levels (line types: solid, dashed, and dotted). The two-way interaction term between VCAM-1 and miR-146a-5p was highly significant (β = −0.0038, SE = 0.0002, $P < 0.001$), indicating a strong negative association with myocardial macrophage infiltration. In contrast, the two-way interaction term between VCAM-1 and SBP did not reach statistical significant (β = 0.00001769, SE = 0.0000204, $P = 0.386$), indicating that the combined effect of VCAM-1 and SBP does not significantly influence macrophage infiltration. The Wald chi-squared test result with two degrees of freedom ($\chi^2 = 299.8$, $P < 0.001$) showed that the slopes of the interaction effects differ significantly from each other.

DISCUSSION

In this study, we uncovered distinct patterns of miRNA regulation associated with hypertensive cardiac pathology in male and female SHRs compared with normotensive WKY. Hypertensive rats had established concentric LVH, and impaired systolic and diastolic functions as well as increased perivascular and interstitial cardiac fibrosis. In addition, hypertensive rats showed endothelial activation and vascular permeability indexed by the increased circulating concentrations of VCAM-1, transendothelial macrophage infiltration

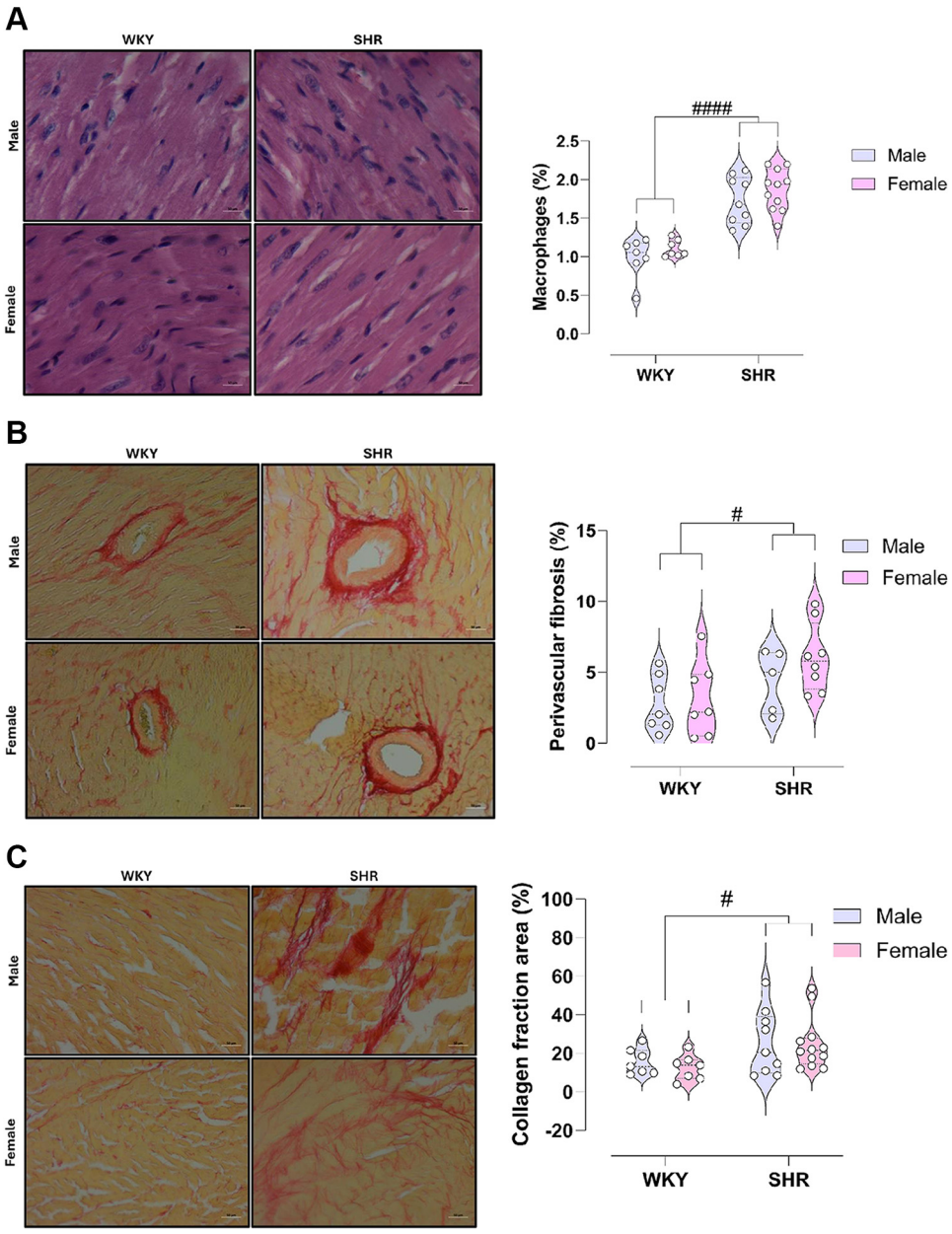

Figure 3. *A*: representative micrographs illustrating myocardial macrophage infiltration in H&E-stained left ventricular tissue sections from male and female WKYs and SHRs (scale bar = 50 μm). Two-way ANOVA with Tukey's post hoc test. *####P* < 0.0001. *B*: representative micrographs illustrating coronary perivascular fibrosis in Sirius red-stained left ventricular tissue sections from male and female WKYs and SHRs (scale bar = 50 μm). Two-way ANOVA with Tukey's post hoc test. *#P* < 0.05. *C*: representative micrographs illustrating myocardial interstitial fibrosis in Sirius red-stained left ventricular tissue sections from male and female WKYs and SHRs (scale bar = 50 μm). Two-way ANOVA with Tukey's post hoc test. *#P* < 0.05. H&E, hematoxylin and eosin; SHR, spontaneously hypertensive rat; WKY, Wistar Kyoto rat.

into cardiac tissue, and increased gene expression of the negative regulator of NF-κB signaling (*NFKBIA*) and oxidative stress (*SOD2*). Female rats exhibited increased LV growth, increased relative mRNA expression of profibrotic genes, and a heightened proinflammatory state. We showed that cardiomyocyte expression of miR-146a-5p was upregulated in the hypertensive heart, whereas miR-155-5p expression was downregulated in female rats. Cardiomyocyte expression of miR-155-5p was positively associated with absolute heart, LV, kidney masses, as well as stroke volume. MiR-146a-5p was positively associated with circulating concentrations of VCAM-1 independently of increases in systolic blood pressure and associated with indices of concentric LVH, diastolic function, and reactive fibrosis. In moderation analyses, increasing expression of miR-146a-5p reversed the relationship between VCAM-1 and macrophage infiltration and the lack of a significant interaction effect between VCAM-1 and SBP suggests that VCAM-1 and SBP may not have a combined effect on macrophage infiltration. Our data may offer novel mechanistic insights into the role of ncRNAs in the development of physiological and pathophysiological cardiac remodeling.

LVH is an adaptive response to chronic hypertension, triggered by pressure overload to counteract increased wall stress (5, 36). The present study is consistent with previous reports (1, 37), showing that 7-mo-old SHR had established concentric LVH, as evidenced by the increased LVPWTd, RWT, and normalized heart and LV masses. Although there is a paucity of literature, miRNAs have gained attention as potential mediators of LVH in pressure overload conditions, regulating cardiac remodeling and hypertrophic signaling

Table 3. *Gene expression in the left ventricular tissue of male and female WKYs and SHRs*

	Male		Female		*P* Value		
	WKY (n = 7)	SHR (n = 7)	WKY (n = 9)	SHR (n = 9)	Strain	Sex	Interaction
Inflammation							
NFKBIA	1.04 ± 0.48	1.49 ± 0.49	1.07 ± 0.25	1.32 ± 0.41	**0.024**	0.634	0.504
IL-1β	1.37 ± 0.65	1.30 ± 0.29	0.88 ± 0.39	1.99 ± 2.31	0.301	0.849	0.240
PTX-3	1.43 ± 2.04	1.45 ± 1.52	2.39 ± 1.50	3.28 ± 1.94	0.484	**0.037**	0.501
Fibrosis							
Col1a	0.61 ± 0.69	0.91 ± 0.56	2.40 ± 1.68	3.10 ± 1.20	0.235	**<0.0001**	0.631
Col3a	1.04 ± 0.58	1.11 ± 0.43	1.18 ± 0.47	0.94 ± 0.40	0.655	0.941	0.428
Col1a/Col3a	1.04 ± 1.33	0.83 ± 0.62	2.07 ± 1.97	3.48 ± 2.12	0.365	**0.0094**	0.226
LOX1	0.63 ± 0.80	1.12 ± 0.90	2.62 ± 1.91	3.90 ± 2.21	0.159	**0.0006**	0.522
Apoptosis							
RUNX-1	0.59 ± 0.55	0.94 ± 0.64	3.48 ± 1.57	4.00 ± 2.64	0.520	**0.0002**	0.893
Oxidative stress							
SOD2	0.98 ± 0.09	1.16 ± 0.17	1.02 ± 0.06	1.16 ± 0.12	**0.001**	0.628	0.645

Data expressed as means ± SD; 2-way ANOVA with Tukey's post hoc test. Boldface indicates statistically significant effects. Col1a, collagen type-I; Col3a, collagen type-III; IL-1β, interleukin-1β; LOX1, lysyl oxidase 1; NFKBIA, nuclear factor of kappa light polypeptide gene enhancer in B-cells inhibitor alpha; PTX-3, pentaxin-3; RUNX1, runt related transcription factor 1; SHR, spontaneously hypertensive rats; SOD2, superoxide dismutase 2; WKY, Wistar Kyoto rats.

pathways. One previous study reported that miR-155-5p and miR-29b-5p expression are reduced in the pressure overload-induced hypertrophic heart and silencing of these miRNAs may induce cardioprotective effects (27). In the present study, the cardiomyocyte expression of miR-29b-5p and miR-155-5p did not differ between SHR and WKY. However, consistent with a study in a rodent model of pressure overload-induced LVH (18), the present study showed upregulation of miR-146a-5p in the LV of SHR. In addition, miR-146a-5p exhibits the most robust and diverse associations with several key parameters related to LVH (RWT, LVPWTd, and normalized heart and LV masses) and diastolic function (e′) as well as an index of endothelial activation and vascular permeability (circulating VCAM-1 concentration), markers of cardiac inflammation (macrophage infiltration, SOD2, and IkBα), and histological assessment of myocardial fibrosis. The diverse and significant correlations of miR-146a-5p with these parameters suggest that miR-146a-5p may be involved in inflammatory signaling and oxidative stress related to structural remodeling.

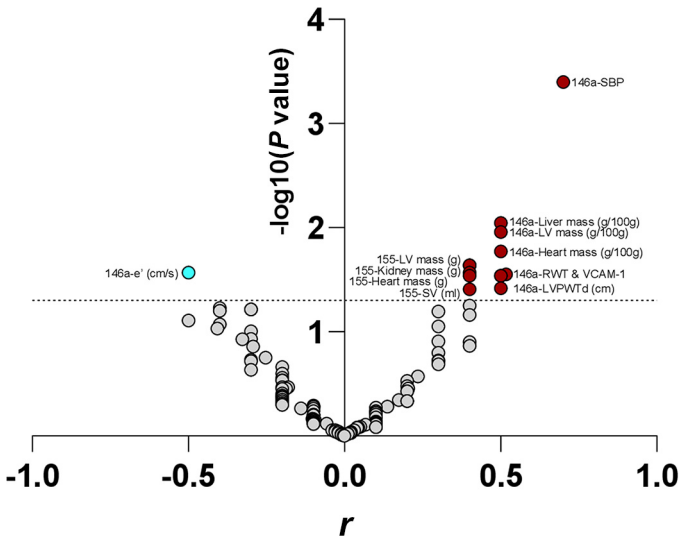

Figure 4. A volcano plot depicting associations between the three microRNAs (miR-146a-5p, miR-155-5p, and miR-29b-5p) and cardiovascular parameters, gene expression in left ventricular tissue, and circulating concentrations of inflammatory markers. The *x*-axis displays Pearson's correlation coefficient (*r*), whereas the *y*-axis shows the −log10(*P* value). Points above the horizontal dashed line [−log10(*P* value) = 1.30, equivalent to $P = 0.05$] indicate statistically significant correlations. Red markers highlight significant positive correlations, particularly involving miR-146a-5p (e.g., SBP, RWT, LVPWTd, and normalized liver mass, LV mass, and heart mass). Parameters associated with miR-155-5p (e.g., absolute LV mass, kidney mass, heart mass, and SV) are also highlighted in red. The turquoise marker represents a significant negative correlation between miR-146a-5p and e′ (cm/s). LV, left ventricular; LVPWTd, LV posterior wall thickness in diastole; RWT, relative wall thickness; SBP, systolic blood pressure.

One mechanism whereby miR-146a-5p has been suggested to be involved in the hypertrophic response is through inflammation-induced fibrosis of the myocardium (28, 38). In high-grade inflammatory conditions, miR-146a-5p directly targets key adaptor molecules *IRAK1* and *TRAF6* involved in the TLR/NF-κB signaling (20). However, in the present study, the concentrations of proinflammatory markers were similar between SHR and WKY. Limited evidence exists to suggest that SHR is a model of low-grade systemic inflammation (39). This suggests that the hypertension-induced cardiac remodeling and dysfunction in SHR may depend on localized rather than systemic inflammation. Indeed, recent evidence indicates that localized inflammation may contribute to the development of concentric LVH in SHR (40), likely due to immune cell infiltration into myocardial tissue. In the present study, the elevated circulating concentrations of VCAM-1 in SHR suggest increased endothelial activation (41, 42), which is permissive to extravasation of monocytes into the myocardium (43). In this respect, VCAM-1 mediates monocyte adhesion to the endothelium and subsequent transendothelial migration into cardiac tissue (44), which may contribute to the observed increase in myocardial macrophage infiltration in SHRs. Interestingly, miR-146a-5p was still associated with VCAM-1 even when adjusted for SBP, suggesting that endothelial activation and vascular permeabilization may result in miRNA-146a-5p activation. Indeed, increasing expression levels of miR-146a-5p, but not SBP, reversed the relationship between VCAM-1 and macrophage infiltration.

The infiltrating macrophages have been shown to predominantly polarize toward the proinflammatory M1 phenotype

Table 4. *Associations between microRNAs and hemodynamic, gravimetric, echocardiographic parameters showing left ventricular geometry, diastolic, and systolic function, inflammatory, and fibrotic markers in male and female normotensive WKY and SHR*

	miR-146a-5p	miR-155-5p	miR-29b-5p
	r (*P*)	*r* (*P*)	*r* (*P*)
Hemodynamic			
SBP	**0.7 (0.0004)**	0.1 (0.575)	0.1 (0.759)
DBP	**0.5 (0.029)**	−0.1 (0.721)	0.2 (0.373)
Gravimetric			
Heart mass, g	0.2 (0.333)	**0.4 (0.029)**	−0.02 (0.908)
Heart mass, g/100 g	**0.5 (0.017)**	−0.3 (0.061)	−0.0001 (0.999)
LV mass, g	0.3 (0.124)	**0.4 (0.023)**	0.04 (0.831)
LV mass, g/100 g	**0.5 (0.011)**	−0.2 (0.339)	0.1 (0.745)
Kidney mass, g	−0.1 (0.751)	**0.4 (0.023)**	−0.1 (0.623)
Kidney mass, g/100 g	0.04 (0.837)	−0.2 (0.218)	−0.2 (0.354)
Liver mass, g	0.3 (0.205)	0.3 (0.064)	−0.02 (0.939)
Liver mass, g/100 g	**0.5 (0.009)**	−0.3 (0.061)	0.05 (0.816)
LV geometry			
LVIDs, cm	−0.01 (0.962)	0.01 (0.948)	−0.2 (0.292)
LVIDd, cm	**−0.4 (0.059)**	0.3 (0.089)	−0.2 (0.465)
IVSTs, cm	0.02 (0.918)	0.3 (0.159)	0.1 (0.821)
IVSTd, cm	0.2 (0.462)	−0.1 (0.707)	−0.1 (0.575)
LVPWTs, cm	0.4 (0.126)	−0.1 (0.550)	0.1 (0.660)
LVPWTd, cm	**0.5 (0.038)**	−0.2 (0.410)	−0.04 (0.880)
RWT	**0.5 (0.029)**	−0.2 (0.389)	0.1 (0.625)
LV systolic function			
Stroke volume, mL	−0.4 (0.085)	**0.4 (0.039)**	0.03 (0.882)
endFS, %	−0.2 (0.500)	0.2 (0.461)	−0.01 (0.970)
midFS, %	−0.5 (0.078)	0.3 (0.189)	−0.2 (0.449)
LV diastolic function			
e′, cm/s	**−0.5 (0.027)**	−0.1 (0.633)	−0.1 (0.512)
a′, cm/s	−0.4 (0.063)	0.1 (0.772)	0.1 (0.729)
e′/a′	0.02 (0.935)	−0.1 (0.522)	−0.3 (0.231)
E, cm/s	0.4 (0.136)	−0.1 (0.741)	−0.2 (0.294)
A, cm/s	0.4 (0.069)	−0.01 (0.975)	−0.3 (0.185)
E/A	−0.1 (0.689)	−0.03 (0.882)	0.3 (0.191)
E/e′	0.4 (0.056)	−0.03 (0.906)	−0.2 (0.419)
Inflammation			
CRP, ng/mL	−0.1 (0.526)	−0.2 (0.251)	−0.1 (0.766)
IL-6, ng/mL	0.1 (0.601)	−0.2 (0.277)	0.1 (0.581)
TNF-α, pg/mL	−0.1 (0.766)	−0.3 (0.192)	0.2 (0.296)
Fibrosis			
Col1a mRNA	0.1 (0.759)	−0.3 (0.099)	−0.1 (0.752)
Col3a mRNA	0.1 (0.825)	−0.2 (0.504)	−0.01 (0.956)
Col1a/Col3a ratio	0.01 (0.959)	−0.2 (0.428)	−0.2 (0.483)
LOX1 mRNA	0.1 (0.536)	−0.3 (0.117)	−0.003 (0.988)
Collagen fraction area, %	**0.4 (0.027)**	−0.1 (0.629)	0.2 (0.372)

Organ masses were normalized to body mass and expressed as g/100 g. Pearson's correlation analyses. Data expressed as correlation coefficients with corresponding *P* values; *r* (*P*). Significant associations are indicated in bold. A, maximum late mitral inflow velocity; a′, late peak tissue lengthening velocity at lateral mitral annulus; Col1a, collagen type 1; Col3a, collagen type 3; CRP, C-reactive protein; E, maximum early mitral inflow velocity; E/A, E/e′, early diastolic mitral inflow to tissue lengthening velocity at lateral mitral annulus; E/A, early to late diastolic filling velocity ratio; e′, early peak tissue lengthening velocity at lateral mitral annulus; e′/a′, early to late peak tissue lengthening velocity ratio; endFS, endocardial fractional shortening; IL-6, interleukin-6; IVSTd, interventricular septal thickness in diastole; IVSTs, interventricular septal thickness in systole; LOX1, lysyl oxidase 1; LV, left ventricular; LVIDd, left ventricular internal diameter in diastole; LVIDs, left ventricular internal diameter in systole; LVPWTd, left ventricular posterior wall thickness in diastole; LVPWTs, left ventricular posterior wall thickness in systole; midFS, midwall fractional shortening; RWT, relative wall thickness; SBP, systolic blood pressure; SHR, spontaneously hypertensive rats; SV, stroke volume; TNF-α, tumor necrosis factor-α; WKY, Wistar Kyoto rats.

(45), a process likely modulated by miR-146a-5p via regulation of the *NF-κB* pathway (46). MiR-146a-5p has been shown to target key components of the *NF-κB* pathway, including *NFKBIA*, which encodes the negative regulator IκBα (47). In the present study, elevated *NFKBIA* expression in SHRs suggests a compensatory mechanism to counterbalance hyperactivated *NF-κB* signaling (48). In line with the involvement of miR-146a-5p as a countermechanism, we observed similar *IL-1β* expression in SHR compared with WKY. This may suggest a dampened macrophage-derived myocardial inflammation. Oxidative stress is another key contributor to hypertensive cardiac remodeling (49). The increased mRNA expression of *SOD2*, which encodes a key antioxidant enzyme, in the myocardium of SHRs reflects a compensatory response to heightened oxidative stress (50). In this regard, miR-146a-5p may modulate redox homeostasis (51). The miR-146a-5p-mediated regulatory network on *SOD2* expression links it to redox imbalance (52), as dysregulation may compromise antioxidant

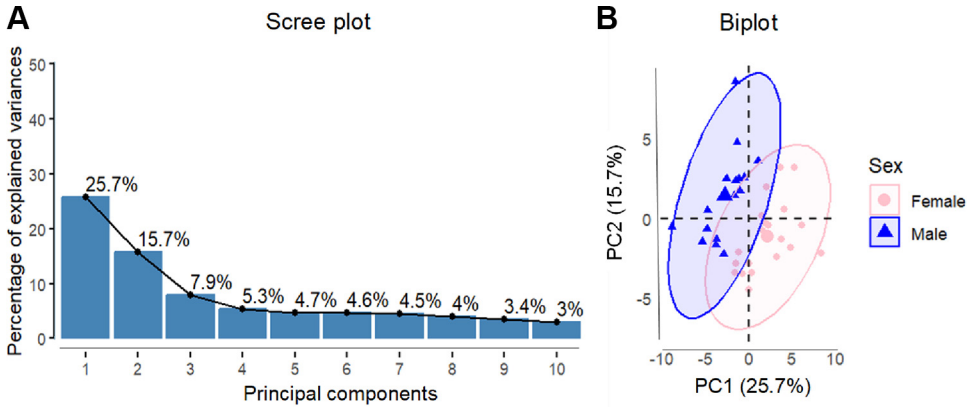

Figure 5. *A* and *B*: an eigenvalue scree plot (*A*) depicting PCA. When disaggregated by sex, sample clustering was observed in the biplot (*B*), and a PERMANOVA test revealed highly significant sex-specific differences in PCA scores (Pillai's Trace = 0.71596, $P < 0.001$). The ellipses (95% CI) represent the Euclidean space within which the data points from each sex are expected to fall. Within each of the ellipses, the centroid reflects the mean location of sex in the Euclidean space. PCA, principal component analysis; PERMANOVA, permutational multivariate analysis of variance.

defenses (53), which drives the apoptotic cascade. Apoptosis further contributes to myocardial remodeling by reducing cardiomyocyte density, promoting cardiomyocyte slippage, and enhancing extracellular matrix deposition to compensate for structural deficits (54). This cascade ultimately drives the transition from compensated hypertrophy to maladaptive remodeling characterized by ventricular dilation and fibrosis.

Given the pleiotropic nature of miRNAs, it is not inconceivable that miR-146a-5p may influence many other pathological processes. We postulate that posttranscriptional regulation may potentially impact mRNA stability (55), RNA binding proteins (56), collagen processing, or translational efficiency in SHRs (57), leading to higher protein levels in the LV without changes in mRNA expression. However, these mechanistic insights could not be gleaned from the present investigation. Elevated blood pressure may drive both perivascular and interstitial fibrosis in SHRs, with the fibrosis following the myocardial wall stress gradient from perivascular regions encroaching into the interstitium (58). This gradient reflects higher wall stress adjacent to the vasculature due to increased pressure load, which perpetuates inflammation, and fibroblast activation (59). The interplay between miR-146a-5p-mediated inflammation and the mechanical stress environment underscores its critical role in hypertensive cardiac remodeling.

In addition to strain-specific expression, miRNAs may have broad effects on downstream signaling pathways in a sex-specific manner (60, 61). The observed clustering by sex in the PCA biplot indicates that males and females can be differentiated based on their physiological profiles, as captured by the contributing variables, reinforcing the idea that biological sex is a key determinant of variability in the measured parameters. In the present study, miR-146a-5p and miR-29b-5p expression did not differ between the sexes. However, we showed a downregulation of miR-155-5p in female rats compared with their male counterparts. The sexual dimorphism in the regulation of miR-155-5p expression may be explained by its relative abundance on the 21q21 X chromosome (62) and the estrogen-mediated regulation of its transcription and processing (63). Taken together, the available evidence on the sex-specific differences in miRNA expression is discordant and warrants further exploration.

The relationship between differential cardiomyocyte expression of miRNAs and echocardiographically derived LV dimensions and function was investigated. We observed phenotypic differences indicative of sexual dimorphism,

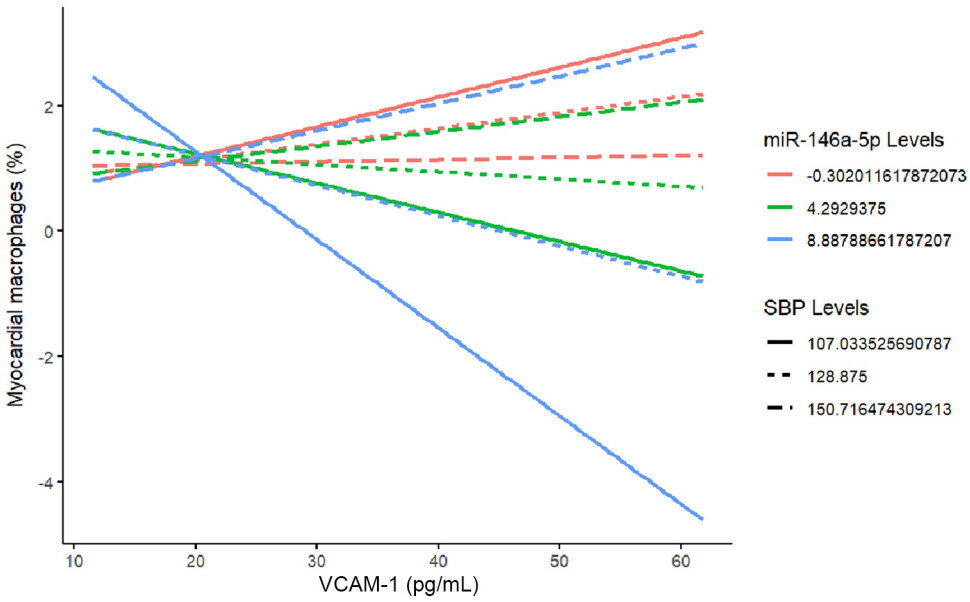

Figure 6. An interaction plot illustrating the relationship between circulating concentrations of VCAM-1 and percent myocardial macrophages, while considering the moderating effects of miR-146a-5p levels (colored lines) and SBP levels (line types: solid, dashed, and dotted). SBP, systolic blood pressure; VCAM-1, vascular cell adhesion molecule-1.

with female rats exhibiting greater normalized heart and LV masses and higher RWT, suggesting that they may have relatively larger hearts and other organs for their body size compared with male rats. One possible reason for the sexual dimorphism may be an adaptation to different physiological demands between male and female rats (64). For this reason, these phenotypic changes may be indicative of increased physiological growth in female rats attributable, in part, to the estrogen-mediated trophic effects on the myocardium (65).

Moreover, sex-specific differences in LV systolic function were observed, with female rats exhibiting lower stroke volume and midFS compared with male rats. We attributed these differences to the Frank–Starling effect, which describes the relationship between end-diastolic volume and stroke volume as a major effect on decreased myocardial contractility (midFS) and cardiac output in female rats (66). Moreover, the lower midFS in female rats contrasts with clinical findings, suggesting that women may have slightly higher midFS (67). These differences may stem from sex-based structural and hemodynamic factors, such as smaller heart size and the influence of estrogen on myocardial function. In addition, variations in myocardial stiffness, chamber compliance, and afterload could affect heart function and disease susceptibility, particularly in conditions like hypertension or heart failure, independent of the microRNAs tested in our study.

In addition, sex as a biological variable may influence the pathogenesis of heart-related conditions at the molecular and cellular levels. In the present study, collagen deposition was greater in female rats that also showed increased expression of circulating levels of proinflammatory markers (CRP, IL-6, and TNF-α), profibrotic genes (*LOX1* mRNA and *Col1a/Col3a* ratio), *RUNX-1*, and *PTX-3*. Numerous lines of evidence have found that females exhibit higher circulating levels of proinflammatory cytokines, such as IL-6 and TNF-α, compared with males (68, 69). Another study investigated the impact of sex hormones on inflammation in SHR, revealing higher expression of proinflammatory markers in the kidneys of female rats (5). However, further research is warranted to establish the direction of causality between sex hormones, systemic inflammation, and fibrotic remodeling in the context of hypertension.

In line with the sexual dimorphism related to the phenotype, the present study shows decreased relative expression of miR-155-5p in female rats that was associated with decreased stroke volume. The observed sexual dimorphism may, at least in part, be attributable to the translational regulation by miR-155-5p of genes involved in these pathways. In this regard, alongside Mann et al. (70), the decreased expression of miR-155-5p may explain the increased circulating levels of proinflammatory markers in female rats. Proinflammatory markers and immune cell infiltration into the myocardium may lead to the activation of cardiac fibroblasts, and excessive deposition of extracellular matrix components (*Col1a*), and increased collagen cross-linking (*LOX1*) (71). MiR-155-5p may clarify the cross talk between inflammation, myocardial fibrosis, and impairment of cardiac function.

Our study focused on miR-146a-5p, miR-155-5p, and miR-29b-5p, potentially overlooking other microRNAs that could contribute to cardiac dysfunction. The mechanisms underlying the observed alterations in miRNA expression profiles and their downstream effects remain incompletely understood, necessitating further mechanistic studies. Notably, miR-146a-5p may be expressed by various cell types, including cardiac fibroblasts and infiltrating macrophages; therefore, our measurement of global LV miRNA levels does not allow us to attribute its expression specifically to cardiomyocytes. As such, although the observed changes in miR-146a-5p levels are associated with the pathology, the specific cellular source of this miRNA remains unclear. Moreover, although our study highlights sex-specific differences in miRNA regulation and cardiac outcomes, the estrous cycle was not evaluated in female rats. Potentially, evaluating the estrous cycle may add granularity when investigating sex-specific differences between the two strains. Also, because of the pleiotropic nature of miRNAs, our study may benefit from assays confirming base complementarity with our target genes. Whether the overexpression of miR-146a-5p in the present study is a cause or a consequence could not be determined. In this regard, rescue experiments involving cardiac-specific silencing or overexpression of miR-146a-5p in SHR may provide crucial information about the upstream regulation of the expression of genes related to the hypertensive and hypertrophic phenotype in SHR. Finally, the relevance of our preclinical findings requires validation in human cohorts to translate these observations into meaningful mechanistic insights in patients with hypertension.

Conclusions

The current study sheds light on the intricate role of miRNAs, particularly miR-146a-5p, miR-155-5p, in the pathogenesis of hypertensive cardiac dysfunction. The relative expression of miR-146a-5p was upregulated in response to pressure overload and was associated with markers of LVH, diastolic dysfunction, and reactive fibrosis. Specifically, miR-146a-5p emerged as a key countermechanism, mitigating VCAM-1-mediated transendothelial macrophage infiltration into the myocardium, inflammation, and oxidative stress by enhancing IκBα and SOD2 expression. Conversely, miR-155-5-p was under-expressed in female rats, consistent with a cardiac phenotype characteristic of sexual dimorphism. By elucidating sex-specific differences in miRNA expression profiles and their associations with cardiac phenotypes in SHR, our data may offer novel insights into the molecular mechanisms underlying hypertensive heart disease. However, further research is warranted to fully elucidate the mechanistic pathways involved and validate our findings in human populations. Ultimately, a deeper understanding of these miRNA-mediated regulatory networks may pave the way for the development of targeted therapeutic strategies to mitigate cardiovascular complications associated with hypertension.

DATA AVAILABILITY

Data will be made available upon reasonable request.

ACKNOWLEDGMENTS

The authors thank Radhini Veerappan and the staff from the Wits Research Animal Facility for the technical assistance.

GRANTS

This work was supported by the South African National Research Foundation grants awarded to S.A.M. (MND210430598430) and F.S.M. (CSRP170502229389).

DISCLOSURES

No conflicts of interest, financial or otherwise, are declared by the authors.

AUTHOR CONTRIBUTIONS

S.A.M. and F.S.M. conceived and designed research; S.A.M., S.G., A.M., K.L.M., A.M.E.M., and F.S.M. performed experiments; S.A.M., A.M., K.L.M., A.M.E.M., and F.S.M. analyzed data; S.A.M., S.G., A.M., L.M., A.M.E.M., and F.S.M. interpreted results of experiments; S.A.M., A.M., and F.S.M. prepared figures; S.A.M., A.M., and F.S.M. drafted manuscript; S.A.M., S.G., A.M., L.M., K.L.M., R.N., A.M.E.M., and F.S.M. edited and revised manuscript; S.A.M., S.G., A.M., L.M., K.L.M., R.N., A.M.E.M., and F.S.M. approved final version of manuscript.

REFERENCES

1. **Mkhize S**, **Manilall A**, **Mokotedi L**, **Gunter S**, **Michel FS.** Involvement of pentraxin-3 in the development of hypertension but not left ventricular hypertrophy in male spontaneously hypertensive rats. *Physiol Rep* 12: e70086, 2024. doi:10.14814/phy2.70086.
2. **Pfeffer TJ**, **Mueller JH**, **Haebel L**, **Erschow S**, **Yalman KC**, **Talbot SR**, **Koenig T**, **Berliner D**, **Zwadlo C**, **Scherr M**, **Hilfiker-Kleiner D**, **Bauersachs J**, **Ricke-Hoch M.** Cabergoline treatment promotes myocardial recovery in peripartum cardiomyopathy. *ESC Heart Fail* 10: 465–477, 2023. doi:10.1002/ehf2.14210.
3. **Drazner MH**, **Rame JE**, **Marino EK**, **Gottdiener JS**, **Kitzman DW**, **Gardin JM**, **Manolio TA**, **Dries DL**, **Siscovick DS.** Increased left ventricular mass is a risk factor for the development of a depressed left ventricular ejection fraction within five years: the Cardiovascular Health Study. *J Am Coll Cardiol* 43: 2207–2215, 2004. doi:10.1016/j.jacc.2003.11.064.
4. **Weinberg EO**, **Thienelt CD**, **Katz SE**, **Bartunek J**, **Tajima M**, **Rohrbach S**, **Douglas PS**, **Lorell BH.** Gender differences in molecular remodeling in pressure overload hypertrophy. *J Am Coll Cardiol* 34: 264–273, 1999. doi:10.1016/s0735-1097(99)00165-5.
5. **Tipton AJ**, **Baban B**, **Sullivan JC.** Female spontaneously hypertensive rats have a compensatory increase in renal regulatory T cells in response to elevations in blood pressure. *Hypertension* 64: 557–564, 2014. doi:10.1161/HYPERTENSIONAHA.114.03512.
6. **Reckelhoff JF.** Gender differences in the regulation of blood pressure. *Hypertension* 37: 1199–1208, 2001. doi:10.1161/01.HYP.37.5.1199.
7. **Lang RM**, **Badano LP**, **Mor-Avi V**, **Afilalo J**, **Armstrong A**, **Ernande L**, **Flachskampf FA**, **Foster E**, **Goldstein SA**, **Kuznetsova T**, **Lancellotti P**, **Muraru D**, **Picard MH**, **Rietzschel ER**, **Rudski L**, **Spencer KT**, **Tsang W**, **Voigt JU.** Recommendations for cardiac chamber quantification by echocardiography in adults: an update from the American Society of Echocardiography and the European Association of Cardiovascular Imaging. *J Am Soc Echocardiogr* 28: 1–39.e14, 2015. doi:10.1016/j.echo.2014.10.003.
8. **Douglas PS**, **Katz SE**, **Weinberg EO**, **Chen MH**, **Bishop SP**, **Lorell BH.** Hypertrophic remodeling: gender differences in the early response to left ventricular pressure overload. *J Am Coll Cardiol* 32: 1118–1125, 1998. doi:10.1016/s0735-1097(98)00347-7.
9. **Reckelhoff JF**, **Zhang H**, **Srivastava K.** Gender differences in development of hypertension in spontaneously hypertensive rats: role of the renin-angiotensin system. *Hypertension* 35: 480–483, 2000. doi:10.1161/01.HYP.35.1.480.
10. **Reckelhoff JF**, **Zhang H**, **Srivastava K**, **Granger JP.** Gender differences in hypertension in spontaneously hypertensive rats: role of androgens and androgen receptor. *Hypertension* 34: 920–923, 1999. doi:10.1161/01.HYP.34.4.920.
11. **Reckelhoff JF**, **Zhang H**, **Granger JP.** Testosterone exacerbates hypertension and reduces pressure-natriuresis in male spontaneously hypertensive rats. *Hypertension* 31: 435–439, 1998. doi:10.1161/01.HYP.31.1.435.
12. **Szczerba E**, **Zajkowska A**, **Bochowicz A**, **Pankiewicz K**, **Szewczyk G**, **Opolski G**, **Maciejewski T**, **Małecki M**, **Fijałkowska A.** Downregulated expression of microRNAs associated with cardiac hypertrophy and fibrosis in physiological pregnancy and the association with echocardiographically-evaluated myocardial function. *Biomed Rep* 13: 41, 2020. doi:10.3892/br.2020.1348.
13. **Hirai K**, **Ousaka D**, **Fukushima Y**, **Kondo M**, **Eitoku T**, **Shigemitsu Y**, **Hara M**, **Baba K**, **Iwasaki T**, **Kasahara S**, **Ohtsuki S**, **Oh H.** Cardiosphere-derived exosomal microRNAs for myocardial repair in pediatric dilated cardiomyopathy. *Sci Transl Med* 12: eabb3336, 2020. doi:10.1126/scitranslmed.abb3336.
14. **Sanchis-Gomar F**, **Arnau-Moyano M**, **Daimiel L**, **Lippi G**, **Leischik R**, **Vallecillo N**, **Yvert T**, **Jiménez SL**, **Santiago C**, **Pareja-Galeano H.** Circulating microRNAs fluctuations in exercise-induced cardiac remodeling: a systematic review. *Am J Transl Res* 13: 13298–13309, 2021.
15. **Täubel J**, **Hauke W**, **Rump S**, **Viereck J**, **Batkai S**, **Poetzsch J**, **Rode L**, **Weigt H**, **Genschel C**, **Lorch U**, **Theek C**, **Levin AA**, **Bauersachs J**, **Solomon SD**, **Thum T.** Novel antisense therapy targeting microRNA-132 in patients with heart failure: results of a first-in-human phase 1b randomized, double-blind, placebo-controlled study. *Eur Heart J* 42: 178–188, 2021. doi:10.1093/eurheartj/ehaa898.
16. **Kaneko M**, **Satomi T**, **Fujiwara S**, **Uchiyama H**, **Kusumoto K**, **Nishimoto T.** AT1 receptor blocker azilsartan medoxomil normalizes plasma miR-146a and miR-342-3p in a murine heart failure model. *Biomarkers* 22: 253–260, 2017. doi:10.1080/1354750X.2016.1204001.
17. **García R**, **Salido-Medina AB**, **Gil A**, **Merino D**, **Gómez J**, **Villar AV**, **González-Vílchez F**, **Hurlé MA**, **Nistal JF.** Sex-specific regulation of miR-29b in the myocardium under pressure overload is associated with differential molecular, structural and functional remodeling patterns in mice and patients with aortic stenosis. *Cells* 9: 833, 2020. doi:10.3390/cells9040833.
18. **Heggermont WA**, **Papageorgiou A-P**, **Quaegebeur A**, **Deckx S**, **Carai P**, **Verhesen W**, **Eelen G**, **Schoors S**, **van Leeuwen R**, **Alekseev S**, **Elzenaar I**, **Vinckier S**, **Pokreisz P**, **Walravens AS**, **Gijsbers R**, **Van Den Haute C**, **Nickel A**, **Schroen B**, **van Bilsen M**, **Janssens S**, **Maack C**, **Pinto Y**, **Carmeliet P**, **Heymans S.** Inhibition of MicroRNA-146a and overexpression of its target dihydrolipoyl succinyltransferase protect against pressure overload-induced cardiac hypertrophy and dysfunction. *Circulation* 136: 747–761, 2017. doi:10.1161/CIRCULATIONAHA.116.024171.
19. **Rasoulinejad SA**, **Akbari A**, **Nasiri K.** Interaction of miR-146a-5p with oxidative stress and inflammation in complications of type 2 diabetes mellitus in male rats: anti-oxidant and anti-inflammatory protection strategies in type 2 diabetic retinopathy. *Iran J Basic Med Sci* 24: 1078–1086, 2021. doi:10.22038/IJBMS.2021.56958.12706.
20. **An R**, **Feng J**, **Xi C**, **Xu J**, **Sun L.** miR-146a attenuates sepsis-induced myocardial dysfunction by suppressing IRAK1 and TRAF6 via targeting ErbB4 expression. *Oxid Med Cell Longev* 2018: 7163057, 2018. doi:10.1155/2018/7163057.
21. **Tang Y**, **Wang YX**, **Zhan YL**, **Liu YF**, **Wu GP**, **Wen LD.** Circular RNA Pum_0014 targets miR-146a-5p/NF2 axis to regulate VEGF/PAK1 pathway and reduce H2O2-induced cardiomyocyte apoptosis. *Altern Ther Health Med* AT9392, 2024.
22. **Pan JA**, **Tang Y**, **Yu JY**, **Zhang H**, **Zhang JF**, **Wang CQ**, **Gu J.** miR-146a attenuates apoptosis and modulates autophagy by targeting TAF9b/P53 pathway in doxorubicin-induced cardiotoxicity. *Cell Death Dis* 10: 668, 2019. doi:10.1038/s41419-019-1901-x.
23. **Zhang Y**, **Huang XR**, **Wei LH**, **Chung AC**, **Yu CM**, **Lan HY.** miR-29b as a therapeutic agent for angiotensin II-induced cardiac fibrosis by targeting TGF-beta/Smad3 signaling. *Mol Ther* 22: 974–985, 2014. doi:10.1038/mt.2014.25.
24. **Thum T**, **Gross C**, **Fiedler J**, **Fischer T**, **Kissler S**, **Bussen M**, **Galuppo P**, **Just S**, **Rottbauer W**, **Frantz S**, **Castoldi M**, **Soutschek J**, **Koteliansky V**, **Rosenwald A**, **Basson MA**, **Licht JD**, **Pena JT**, **Rouhanifard SH**, **Muckenthaler MU**, **Tuschl T**, **Martin GR**, **Bauersachs J**, **Engelhardt S.** MicroRNA-21 contributes to myocardial disease by stimulating MAP kinase signalling in fibroblasts. *Nature* 456: 980–984, 2008. doi:10.1038/nature07511.

25. **Silva J**, **da Costa Martins PA.** Non-coding RNAs in the therapeutic landscape of pathological cardiac hypertrophy. *Cells* 11: 1805, 2022. doi:10.3390/cells11111805.
26. **Oh JG**, **Watanabe S**, **Lee A**, **Gorski PA**, **Lee P**, **Jeong D**, **Liang L**, **Liang Y**, **Baccarini A**, **Sahoo S**, **Brown BD**, **Hajjar RJ**, **Kho C.** miR-146a suppresses SUMO1 expression and induces cardiac dysfunction in maladaptive hypertrophy. *Circ Res* 123: 673–685, 2018. doi:10.1161/CIRCRESAHA.118.312751.
27. **Seok HY**, **Chen J**, **Kataoka M**, **Huang ZP**, **Ding J**, **Yan J**, **Hu X**, **Wang DZ.** Loss of microRNA-155 protects the heart from pathological cardiac hypertrophy. *Circ Res* 114: 1585–1595, 2014. doi:10.1161/CIRCRESAHA.114.303784.
28. **Feng B**, **Chen S**, **Gordon AD**, **Chakrabarti S.** miR-146a mediates inflammatory changes and fibrosis in the heart in diabetes. *J Mol Cell Cardiol* 105: 70–76, 2017. doi:10.1016/j.yjmcc.2017.03.002.
29. **Hu J**, **Huang S**, **Liu X**, **Zhang Y**, **Wei S**, **Hu X.** miR-155: an important role in inflammation response. *J Immunol Res* 2022: 7437281, 2022. doi:10.1155/2022/7437281.
30. **Gilyazova I**, **Asadullina D**, **Kagirova E**, **Sikka R**, **Mustafin A**, **Ivanova E**, **Bakhtiyarova K**, **Gilyazova G**, **Gupta S**, **Khusnutdinova E**, **Gupta H**, **Pavlov V.** MiRNA-146a-A key player in immunity and diseases. *Int J Mol Sci* 24: 12767, 2023. doi:10.3390/ijms241612767.
31. **Percie Du Sert N**, **Ahluwalia A**, **Alam S**, **Avey MT**, **Baker M**, **Browne WJ**, **Clark A**, **Cuthill IC**, **Dirnagl U**, **Emerson M**, **Garner P**, **Holgate ST**, **Howells DW**, **Hurst V**, **Karp NA**, **Lazic SE**, **Lidster K**, **MacCallum CJ**, **Macleod M**, **Pearl EJ**, **Petersen OH**, **Rawle F**, **Reynolds P**, **Rooney K**, **Sena ES**, **Silberberg SD**, **Steckler T**, **Würbel H.** Reporting animal research: explanation and elaboration for the ARRIVE guidelines 2.0. *PLoS Biol* 18: e3000411, 2020. doi:10.1371/journal.pbio.3000411.
32. **Al-Gburi S**, **Deussen AJ**, **Galli R**, **Muders MH**, **Zatschler B**, **Neisser A**, **Müller B**, **Kopaliani I.** Sex-specific differences in age-dependent progression of aortic dysfunction and related cardiac remodeling in spontaneously hypertensive rats. *Am J Physiol Regul Integr Comp Physiol* 312: R835–R849, 2017. doi:10.1152/ajpregu.00231.2016.
33. **Mokotedi L**, **Michel FS**, **Mogane C**, **Gomes M**, **Woodiwiss AJ**, **Norton GR**, **Millen AME.** Associations of inflammatory markers with impaired left ventricular diastolic and systolic function in collagen-induced arthritis. *PLoS One* 15: e0230657, 2020. doi:10.1371/journal.pone.0230657.
34. **Sahn DJ**, **DeMaria A**, **Kisslo J**, **Weyman A.** Recommendations regarding quantitation in M-Mode echocardiography: results of a survey of echocardiographic measurements. *Circulation* 58: 1072–1083, 1978. doi:10.1161/01.CIR.58.6.1072.
35. **Livak KJ**, **Schmittgen TD.** Analysis of relative gene expression data using real-time quantitative PCR and the $2^{-\Delta\Delta CT}$ Method. *Methods* 25: 402–408, 2001. doi:10.1006/meth.2001.1262.
36. **Gosse P.** Left ventricular hypertrophy as a predictor of cardiovascular risk. *J Hypertens Suppl* 23: S27–S33, 2005. doi:10.1097/01.hjh.0000165625.79933.9a.
37. **Hawlitschek C**, **Brendel J**, **Gabriel P**, **Schierle K**, **Salameh A**, **Zimmer HG**, **Rassler B.** How effective is a late-onset antihypertensive treatment? studies with captopril as monotherapy and in combination with nifedipine in old spontaneously hypertensive rats. *Biomedicines* 10: 1964, 2022. doi:10.3390/biomedicines10081964.
38. **Halkein J**, **Tabruyn SP**, **Ricke-Hoch M**, **Haghikia A**, **Nguyen NQ**, **Scherr M**, **Castermans K**, **Malvaux L**, **Lambert V**, **Thiry M**, **Sliwa K**, **Noel A**, **Martial JA**, **Hilfiker-Kleiner D**, **Struman I.** MicroRNA-146a is a therapeutic target and biomarker for peripartum cardiomyopathy. *J Clin Invest* 123: 2143–2154, 2013. doi:10.1172/JCI64365.
39. **Dinh QN**, **Drummond GR**, **Sobey CG**, **Chrissobolis S.** Roles of inflammation, oxidative stress, and vascular dysfunction in hypertension. *Biomed Res Int* 2014: 406960, 2014. doi:10.1155/2014/406960.
40. **Li L**, **Yi-Ming W**, **Li ZZ**, **Zhao L**, **Yu YS**, **Li DJ**, **Xia CY**, **Liu JG**, **Su DF.** Local RAS and inflammatory factors are involved in cardiovascular hypertrophy in spontaneously hypertensive rats. *Pharmacol Res* 58: 196–201, 2008. doi:10.1016/j.phrs.2008.06.009.
41. **Usui T**, **Okada M**, **Hara Y**, **Yamawaki H.** Death-associated protein kinase 3 mediates vascular inflammation and development of hypertension in spontaneously hypertensive rats. *Hypertension* 60: 1031–1039, 2012. doi:10.1161/HYPERTENSIONAHA.112.200337.
42. **McCarron RM**, **Wang L**, **Siren AL**, **Spatz M**, **Hallenbeck JM.** Monocyte adhesion to cerebromicrovascular endothelial cells derived from hypertensive and normotensive rats. *Am J Physiol Heart Circ Physiol* 267: H2491–H2497, 1994. doi:10.1152/ajpheart.1994.267.6.H2491.
43. **Schmitz B**, **Vischer P**, **Brand E**, **Schmidt-Petersen K**, **Korb-Pap A**, **Guske K**, **Nedele J**, **Schelleckes M**, **Hillen J**, **Rötrige A**, **Simmet T**, **Paul M**, **Cambien F**, **Brand SM.** Increased monocyte adhesion by endothelial expression of VCAM-1 missense variation in vitro. *Atherosclerosis* 230: 185–190, 2013. doi:10.1016/j.atherosclerosis.2013.07.039.
44. **Medrano-Bosch M**, **Simón-Codina B**, **Jiménez W**, **Edelman ER**, **Melgar-Lesmes P.** Monocyte-endothelial cell interactions in vascular and tissue remodeling. *Front Immunol* 14: 1196033, 2023. doi:10.3389/fimmu.2023.1196033.
45. **Luo M**, **Zhao F**, **Cheng H**, **Su M**, **Wang Y.** Macrophage polarization: an important role in inflammatory diseases. *Front Immunol* 15: 1352946, 2024. doi:10.3389/fimmu.2024.1352946.
46. **Chen R**, **Zhang H**, **Tang B**, **Luo Y**, **Yang Y**, **Zhong X**, **Chen S**, **Xu X**, **Huang S**, **Liu C.** Macrophages in cardiovascular diseases: molecular mechanisms and therapeutic targets. *Signal Transduct Target Ther* 9: 130, 2024. doi:10.1038/s41392-024-01840-1.
47. **Cuenca-Zamora EJ**, **Guijarro-Carrillo PJ**, **López-Poveda MJ**, **Morales ML**, **Lozano ML**, **Gonzalez-Conejero R**, **Martínez C**, **Teruel-Montoya R**, **Ferrer-Marín F.** miR-146a-/- mice model reveals that NF-κB inhibition reverts inflammation-driven myelofibrosis-like phenotype. *Am J Hematol* 99: 1326–1337, 2024. doi:10.1002/ajh.27322.
48. **Prescott JA**, **Mitchell JP**, **Cook SJ.** Inhibitory feedback control of NF-κB signalling in health and disease. *Biochem J* 478: 2619–2664, 2021. doi:10.1042/BCJ20210139.
49. **Rababa'h AM**, **Guillory AN**, **Mustafa R**, **Hijjawi T.** Oxidative stress and cardiac remodeling: an updated edge. *Curr Cardiol Rev* 14: 53–59, 2018. doi:10.2174/1573403X14666180111145207.
50. **Sam F**, **Kerstetter DL**, **Pimental DR**, **Mulukutla S**, **Tabaee A**, **Bristow MR**, **Colucci WS**, **Sawyer DB.** Increased reactive oxygen species production and functional alterations in antioxidant enzymes in human failing myocardium. *J Card Fail* 11: 473–480, 2005. doi:10.1016/j.cardfail.2005.01.007.
51. **Dasgupta N**, **Peng Y**, **Tan Z**, **Ciraolo G**, **Wang D**, **Li R.** miRNAs in mtDNA-less cell mitochondria. *Cell Death Discov* 1: 15004, 2015. doi:10.1038/cddiscovery.2015.4.
52. **Zorov DB**, **Juhaszova M**, **Sollott SJ.** Mitochondrial reactive oxygen species (ROS) and ROS-induced ROS release. *Physiol Rev* 94: 909–950, 2014. doi:10.1152/physrev.00026.2013.
53. **Zong Y**, **Li H**, **Liao P**, **Chen L**, **Pan Y**, **Zheng Y**, **Zhang C**, **Liu D**, **Zheng M**, **Gao J.** Mitochondrial dysfunction: mechanisms and advances in therapy. *Signal Transduct Target Ther* 9: 124, 2024. doi:10.1038/s41392-024-01839-8.
54. **Bennett MR.** Apoptosis in the cardiovascular system. *Heart* 87: 480–487, 2002. doi:10.1136/heart.87.5.480.
55. **Nouaille S**, **Mondeil S**, **Finoux AL**, **Moulis C**, **Girbal L**, **Cocaign-Bousquet M.** The stability of an mRNA is influenced by its concentration: a potential physical mechanism to regulate gene expression. *Nucleic Acids Res* 45: 11711–11724, 2017. doi:10.1093/nar/gkx781.
56. **Van Assche E**, **Van Puyvelde S**, **Vanderleyden J**, **Steenackers HP.** RNA-binding proteins involved in post-transcriptional regulation in bacteria. *Front Microbiol* 6: 141, 2015. doi:10.3389/fmicb.2015.00141.
57. **Tuller T**, **Waldman YY**, **Kupiec M**, **Ruppin E.** Translation efficiency is determined by both codon bias and folding energy. *Proc Natl Acad Sci USA* 107: 3645–3650, 2010. doi:10.1073/pnas.0909910107.
58. **Díez J**, **González A**, **Kovacic JC.** Myocardial interstitial fibrosis in nonischemic heart disease, part 3/4: JACC focus seminar. *J Am Coll Cardiol* 75: 2204–2218, 2020. doi:10.1016/j.jacc.2020.03.019.
59. **Torimoto K**, **Elliott K**, **Nakayama Y**, **Yanagisawa H**, **Eguchi S.** Cardiac and perivascular myofibroblasts, matrifibrocytes, and immune fibrocytes in hypertension; commonalities and differences with other cardiovascular diseases. *Cardiovasc Res* 120: 567–580, 2024. doi:10.1093/cvr/cvae044.
60. **Wei C**, **Henderson H**, **Spradley C**, **Li L**, **Kim I-K**, **Kumar S**, **Hong N**, **Arroliga AC**, **Gupta S.** Circulating miRNAs as potential marker for pulmonary hypertension. *PLoS One* 8: e64396, 2013. doi:10.1371/journal.pone.0064396.
61. **Wallace E**, **Morrell NW**, **Yang XD**, **Long L**, **Stevens H**, **Nilsen M**, **Loughlin L**, **Mair KM**, **Baker AH**, **MacLean MR.** A sex-specific microRNA-96/5-hydroxytryptamine 1B axis influences development of pulmonary hypertension. *Am J Respir Crit Care Med* 191: 1432–1442, 2015. doi:10.1164/rccm.201412-2148OC.

62. **Malmhäll C**, **Weidner J**, **Rådinger M.** MicroRNA-155 expression suggests a sex disparity in innate lymphoid cells at the single-cell level. *Cell Mol Immunol* 17: 544–546, 2020. doi:10.1038/s41423-019-0303-4.
63. **Florijn BW**, **Bijkerk R**, **van der Veer EP**, **van Zonneveld AJ.** Gender and cardiovascular disease: are sex-biased microRNA networks a driving force behind heart failure with preserved ejection fraction in women? *Cardiovasc Res* 114: 210–225, 2018. doi:10.1093/cvr/cvx223.
64. **St Pierre SR**, **Peirlinck M**, **Kuhl E.** Sex matters: a comprehensive comparison of female and male hearts. *Front Physiol* 13: 831179, 2022. doi:10.3389/fphys.2022.831179.
65. **Bhupathy P**, **Haines D**, **Leinwand L.** Influence of sex hormones and phytoestrogens on heart disease in men and women. *Womens Health (Lond)* 6: 77–95, 2010. doi:10.2217/whe.09.80.
66. **Pfeffer J**, **Pfeffer M**, **Fletcher P**, **Braunwald E.** Alterations of cardiac performance in rats with established spontaneous hypertension. *Am J Cardiol* 44: 994–998, 1979. doi:10.1016/0002-9149(79)90234-0.
67. **Gerdts E**, **Zabalgoitia M**, **Björnstad H**, **Svendsen TL**, **Devereux RB.** Gender differences in systolic left ventricular function in hypertensive patients with electrocardiographic left ventricular hypertrophy (the LIFE study). *Am J Cardiol* 87: 980–983; A4, 2001. doi:10.1016/s0002-9149(01)01433-3.
68. **Dela Justina V**, **Miguez JSG**, **Priviero F**, **Sullivan JC**, **Giachini FR**, **Webb RC.** Sex differences in molecular mechanisms of cardiovascular aging. *Front Aging* 2: 725884, 2021. doi:10.3389/fragi.2021.725884.
69. **Sullivan JC**, **Pardieck JL**, **Doran D**, **Zhang Y**, **She JX**, **Pollock JS.** Greater fractalkine expression in mesenteric arteries of female spontaneously hypertensive rats compared with males. *Am J Physiol Heart Circ Physiol* 296: H1080–H1088, 2009. doi:10.1152/ajpheart.01093.2008.
70. **Mann M**, **Mehta A**, **Zhao JL**, **Lee K**, **Marinov GK**, **Garcia-Flores Y**, **Lu LF**, **Rudensky AY**, **Baltimore D.** An NF-κB-microRNA regulatory network tunes macrophage inflammatory responses. *Nat Commun* 8: 851, 2017 [Erratum in *Nat Commun* 9: 3338, 2018]. doi:10.1038/s41467-017-00972-z.
71. **Hall C**, **Law JP**, **Reyat JS**, **Cumberland MJ**, **Hang S**, **Vo NTN**, **Raniga K**, **Weston CJ**, **O'Shea C**, **Townend JN**, **Gehmlich K**, **Ferro CJ**, **Denning C**, **Pavlovic D.** Chronic activation of human cardiac fibroblasts in vitro attenuates the reversibility of the myofibroblast phenotype. *Sci Rep* 13: 12137, 2023. doi:10.1038/s41598-023-39369-y.